KINEMATIC ANALYSIS AND OPTIMAL DESIGN OF THE SEPARATION CONVEYOR DEVICE FOR *PANAX NOTOGINSENG* COMBINE HARVESTER

Ibrahim Issa Mohamed ISSA[1,3*], Zhaoguo ZHANG[1,2,3*], Wael EL-KOLALY[4], Altyeb Ali Abaker OMER[5], Faan WANG[2,3], Jie SONG[2,3]

[1] Faculty of Mechanical and Electrical Engineering, Kunming University of Science and Technology, Kunming 650500, China;
[2] Faculty of Modern Agricultural Engineering, Kunming University of Science and Technology, Kunming 650500, China;
[3] Research Center on Mechanization Engineering of Chinese Medicinal Materials in Yunnan Universities, Kunming 650500, China;
[4] Agricultural Engineering Research Institute (AEnRI), Agricultural Research Center (ARC), Ministry of Agriculture, 256 Dokki, Giza, Egypt;
[5] School of Tea and Coffee, Puer University, Puer, China

Corresponding authors: Ibrahim Issa Mohamed Issa, E-mail: ibrahimeisa14@gmail.com,
Zhang Zhaoguo, E-mail: zzg@kust.edu.cn
DOI: https://doi.org/10.35633/inmateh-79-30

***Keywords:** Panax notoginseng; Hilly and Mountainous Areas; Separation Conveyor; EDEM Simulation; SolidWorks*

ABSTRACT
Panax notoginseng is a high-value medicinal rhizome crop widely cultivated in the hilly and mountainous regions of southwest China, where traditional manual harvesting remains labor-intensive and inefficient. To address these challenges, this study focuses on the design, kinematic analysis, optimization, and validation of a separation conveyor device for a self-propelled Panax notoginseng combine harvester. The separation conveyor was developed based on the agronomic characteristics of Panax notoginseng and the mechanical requirements of soil-rhizome separation. A comprehensive methodology integrating theoretical modeling, kinematic and mechanical analysis, coupled discrete element-multibody dynamics (DEM-MBD) simulations using EDEM and RecurDyn, and laboratory experiments was employed. Key operational parameters, including conveyor speed, vibration frequency, and lifting angle, were systematically evaluated through quadratic regression and orthogonal experimental design. Simulation results indicated that effective soil separation could be achieved within 2.25 s, with fine soil particles separating earlier than larger aggregates. Laboratory tests identified optimal parameters of 0.8 m·s⁻¹ conveyor speed, 1.5 Hz vibration frequency, and a 20° lifting angle. Field validation experiments confirmed the reliability of the optimized design, achieving average separation and conveying rates of 96.87% and 96.42%, respectively, with a low rhizome damage rate of 1.88%. The results demonstrate that the proposed separation conveyor provides an effective solution for mechanized harvesting of Panax notoginseng and offers valuable reference for similar rhizome crop harvesters.

INTRODUCTION
Panax notoginseng is unique to southwest China, a well-known rhizome-based traditional Chinese medicine with excellent medicinal and economic value, which removes blood stasis and prevents cardiovascular and cerebrovascular diseases (*Issa et al., 2025c; Jiang et al., 2022; Lin et al., 2022*). Flowers, leaves, stems, and rhizomes can all be used as medicine. Modern medical research has found that *Panax Notoginseng* is rich in saponins, flavonoids, and various amino acids (*Zhou et al., 2010*). It is mainly cultivated in hilly and mountainous areas (*Zhang et al., 2016; Zhaoguo et al., 2023*). *Panax notoginseng* is mainly produced in mountainous and hilly areas such as Yunnan, Guangxi, and Sichuan *(Guiyun and Ying, 2012; Guo Jingjing et al., 2014*). Yunnan Province is located in the southwest of China and has mountainous plateau terrain. 87.21% of Yunnan Province’s land area is located in the 1000~3000m medium altitude area. Mountains, hills, plains, and terraces account for 88.64%, 4.96%, 4.85% and 1.55% of Yunnan Province’s area, respectively. Most of them are hilly and mountainous (*Thomas, 1992*). In recent years, the *Panax notoginseng* industry has entered a stage of large-scale, base-based, and standardized development *(Lihong et al., 2017*). However, *Panax notoginseng* is mainly harvested by traditional manual harvesting, which has low harvesting efficiency, high labor intensity, and is time-consuming and labor-intensive *(Zhenmeng et al., 2018*). Mechanized harvesting of *Panax notoginseng* can reduce farmers' work intensity and improve work efficiency *(Faan et al., 2024*).

Guo Siwei and others designed and developed a self-propelled *Panax notoginseng* combine harvester. The machine consists of an excavator, a primary conveying and separation device, a secondary conveying and separation device, a lifting device, a collection device, a hydraulic transmission system, a control system, and a crawler system. It integrates excavation, separation, conveying, and collection, achieving mechanized harvesting of *Panax notoginseng* and effectively reducing labor intensity (*Siwei, 2024*).

There is limited research on separation conveyor devices for rhizome crop harvesters from research institutes, while most research comes from agricultural machinery manufacturers (*Issa et al., 2025b*). For example, Johnson et al. applied the separation conveyor device to the technology of separation and loading conveyance using a hydraulic system to achieve highly controllable separation and conveying. The American Lockwood company developed a potato harvester that uses two-stage separation and conveying technology to load the harvester into the collection box, thereby improving separation and conveying efficiency *(Yitao et al., 2020*). The Japanese Matsuyama GSA600 harvester uses a rubber conveyor belt to improve durability without damaging rhizome and tuber tissue. The vibration device uses a three-speed adjustable setting to deliver different vibration frequencies for various crops and soil conditions (*Cheng et al., 2023*).

Recent research on conveying and separation devices for rhizome crop harvesters in China has primarily used DEM-MBD coupling simulations to design separation and conveying devices, study the movement of rhizomes and soil during the separation process, and assess the crushing effect *(Chen et al., 2024; Issa et al., 2025a; Wang et al., 2023b; Wang et al., 2023c*). For example, Wei Zhongcai from Shandong University of Science and Technology designed a wave-shaped conveyor suitable for potatoes *(Zhongcai et al., 2020*). To address the issue of high potato damage and skin breakage rates, he analyzed the key factors and structural parameters of the potato-soil separation process, utilizing a dual separation method that combines vibration and wave techniques to reduce these rates; additionally, Wang Feng from Gansu Agricultural University designed a double-layer separation conveyor for Pinellia Ternata, which employed a method of first conveying and then separating, while configuring the separation operation separately to enhance the rhizome-soil separation effect (*Feng, 2022*).

In summary, most rhizome and tuber harvesters in China, especially those for Chinese medicinal materials, have simple structures, small operating widths, and are mostly specialized harvesters for single medicinal materials. The conveying and separation components mainly include bar-type lifting chains, connecting-rod vibrating conveyors, roller conveyor chains, and cylindrical screens. In combination with previous research, the heavy soil in the *Panax notoginseng* planting area makes rhizome and soil separation more difficult, and the *Panax notoginseng* rhizome is rigid. It is challenging to break parameters during the conveying and separation process. Therefore, to ensure the separation of the rhizome and soil.

This study focused on the development and optimization of a separation conveyor for a self-propelled *Panax notoginseng* harvester to improve soil–rhizome separation efficiency. The separation conveyor was designed using computer-aided design tools and analyzed through coupled discrete element and multibody dynamics simulations. EDEM and RecurDyn software were used to simulate the conveying and separation processes and investigate the interactions among soil particles, rhizomes, and conveyor components. Key operating factors, including conveyor speed, vibration frequency, and lifting angle, were systematically evaluated using quadratic regression analysis to identify optimal parameter combinations. Field experiments were conducted to verify the simulation model and assess separation performance under practical operating conditions. The combined simulation and experimental approach provided a scientific basis for optimizing the structure and operating parameters of the separation conveyor system.

MATERIALS AND METHODS

Self-propelled combine harvester structure and working principle

Based on the agronomic conditions for *Panax notoginseng* cultivation in Yunnan and the basic physical parameters of *Panax notoginseng* and the soil, a self-propelled *Panax notoginseng* combine harvester was designed. *Panax notoginseng* is mainly planted in hilly and mountainous areas. Considering the influence of slopes, the entire machine should be smaller to meet the working requirements and deliver excellent performance. At the same time, it should meet the design requirements of relevant national and local standards. The strong adaptability and possibility of the crawler chassis, which can turn around at the end of fields, and adapt to different working conditions. Therefore, this study aims to design key components of a crawler self-propelled *Panax notoginseng* combined harvester to enable joint operations for *Panax notoginseng* excavation, separation, transportation, lifting, collection, and unloading, thereby adapting to small-plot operations in hilly and mountainous areas.

The *Panax notoginseng* combine harvester designed in this research comprises an excavation device, a separation conveyor device, a lifting device, a collection device, an engine, a hydraulic caterpillar chassis, and a wheelhouse, as shown in Figure 1. The entire vehicle utilizes hydraulic control. The engine drives the hydraulic pump, supplying power to the combine harvester. The hydraulic valve group then distributes this power to each system, moving the hydraulic motor and hydraulic cylinder to enable walking and harvesting operations.

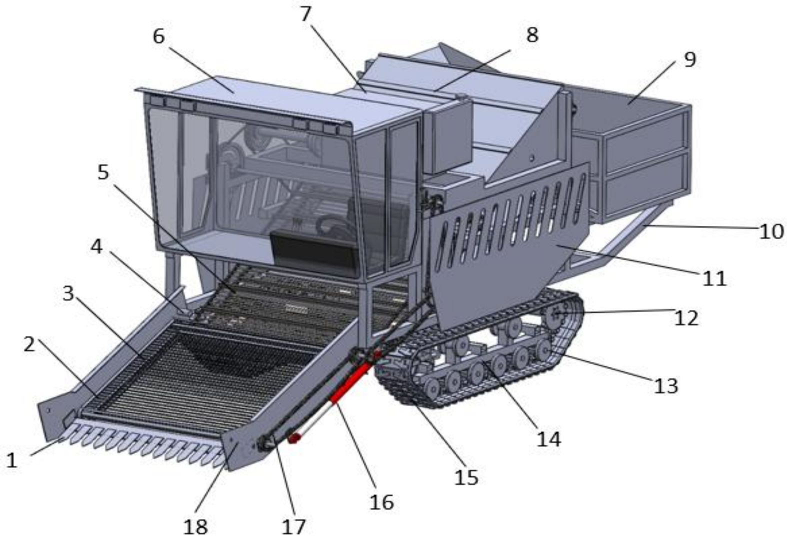

Fig. 1 - Self-propelled *Panax Notoginseng* Combine Harvester

1. Excavation shovel; 2. Separation conveyor; 3. Vibration device; 4. Pillar; 5. Lifting device 6. Wheelhouse; 7. Engine; 8. Lifting device cover 9. Collecting box; 10. Chassis; 11. Frame; 12. Drive wheel; 13. Support wheels; 14. Crawler chassis walking frame; 15. V Rubber tracks; 16. Hydraulic cylinder for collecting box; 17. Transmission chain18. Separation conveyor device frame.

When the *Panax notoginseng* combine harvester is operating, the excavation shovel is aligned with the *Panax notoginseng* ridge and the corresponding height is adjusted to meet the depth and angle of *Panax notoginseng* harvesting; the speed of the separation conveyor and the vibrating wheel are adjusted so that the excavated *Panax notoginseng* rhizome-soil complex can achieve a relatively ideal separation effect during the soil separating operation; the excavation shovel digs and crushes the *Panax notoginseng* rhizome-soil complex to facilitate the subsequent conveying and soil removal process; the separation conveyor is transported backward, and the *Panax notoginseng* rhizome-soil complex is shaken by the vibrating wheel to achieve soil removal; the *Panax notoginseng* after soil removal is thrown from the separation conveyor to the lifting device, and transported upward under the drive of the chain; after reaching the top, it is thrown into the aggregate box to complete the entire harvesting operation; after the collection is completed, the hydraulic cylinder flips it over to complete the unloading operation.

Design and analysis of the separation conveyor device

The separation conveyor is designed to separate soil from rhizomes and transport them. In contrast, the lifting device's primary role is transportation. During operation, the excavation device gathers the rhizome-soil mixture and delivers it to the separation conveyor. Here, soil is removed, and the *Panax notoginseng* rhizomes are conveyed onward. Finally, the cleaned rhizomes, along with any residual soil, are transferred to the lifting device for further transport.

Commonly used conveying devices can be divided into belt conveyor, roller push-type, chain-type lifting, bucket elevator, and throwing wheel type, according to structural form. Among them, the bar-type structure is more suitable for harvesting *Panax notoginseng* rhizome. It is simple to operate and has strong separation performance. It can ensure good conveying capacity at a large lifting angle (*Issa et al., 2020; Xiaohong, 2023*). It mainly includes guide wheels, plum blossom-shaped drive wheels, lifting chains, vibration wheels, driven wheels, and supporting wheels. After *Panax notoginseng* is excavated, it enters the separation conveyor device. During transport, fine impurities are directly deposited on the ridge through the bars. Part or all of the rhizome-soil complex, and large soil blocks, are further separated from the vibration wheel by vibration and then transported to the lifting device of the working components. The three-dimensional model of the separation conveyor components is shown in Figure 2. The primary power source is hydraulic transmission.

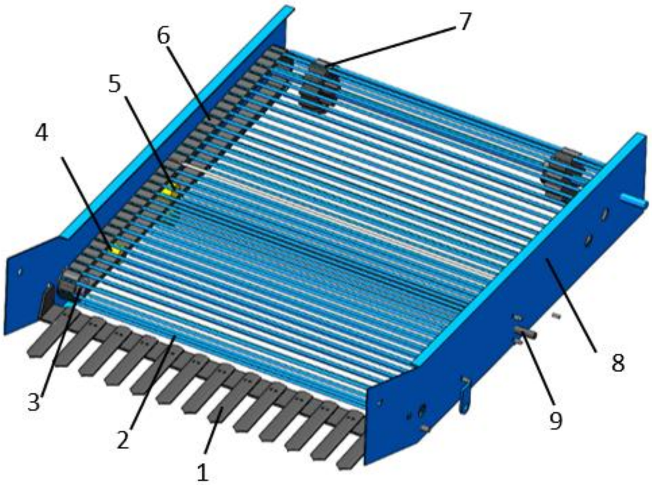

Fig. 2 - Structural diagram of the separation conveyor device

1. Excavation shovel; 2. Rod; 3. Driven wheel; 4. Supporting wheel 5. Vibration device; 6. Separation conveyor belt; 7. Drive wheels; 8. Separation conveyor frame; 9. Vibration device pillar

The working principle is that the excavation device removes the *Panax notoginseng* rhizome-soil complex, and the complex is transported to the separation conveyor device by friction and inertia. The soil is then broken, separated, and dropped by the vibration wheel. Finally, the *Panax notoginseng* is thrown to the lifting device at the rear end of the lifting chain. The main technical parameters are shown in Table 1.

Table 1

Main technical parameters of the separation conveyor device

Parameter	Numerical value
Device diameters (length × wide × Height)	1988×1540×1080 mm
Device weight	410 kg
Number of harvested ridges	1
Working width	1500 mm
Operating speed	≥0.4 m/s
Conveying speed	0.4 ~ 1.0 m/s

According to the previous planting site survey, the working width was determined to be 1500 mm. According to the design requirements of the bar elevator in the Agricultural Machinery Design Manual (*Hongwei, 2024*). The conveyor belt length should be 1200~1500 mm, and the selected length is 1400 mm. The bar gap was determined based on the minimum triaxial dimensions of the *Panax notoginseng* rhizome-soil complex. According to the previous research, the bar diameter was selected as 12 mm, the bar gap was 38 mm, and the bar center distance was 50 mm, as shown in Figure 3.

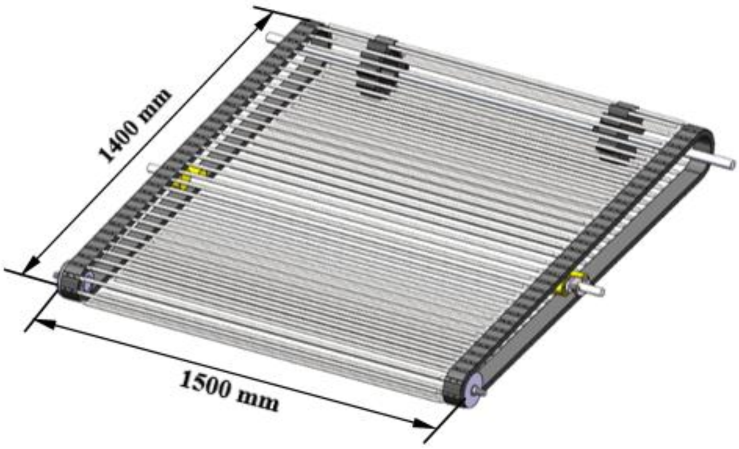

Fig. 3 - Separation conveyor size

On rhizome harvesters in many countries around the world, the distance between the harvester bars on the vibrating screen is 25~28 mm, 40~48 mm in the United States, and 30~40 mm in Japan and South Korea (*Wang et al., 2025; Zhaoguo et al., 2021*). The two-dimensional design scheme of the bar is shown in Fig. 4.

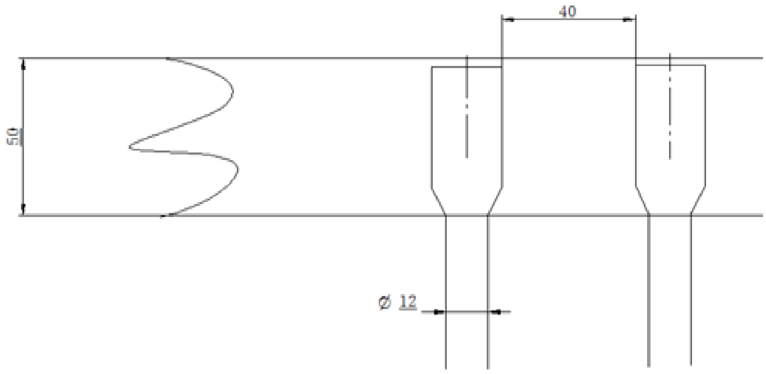

Fig. 4 - Design scheme of the bar

Determination of the drive wheel

The driving wheel is the main working part of the *Panax notoginseng* combined harvester movement transmission. It is also the main power-consumption component, driving the rotation of the entire conveyor belt and the movement of the vibration wheel, driven wheel, and supporting wheel. The actual production of the drive wheel is also complicated. The wheel hub is made of metal material and covered with plum blossom rubber. It is fixed on the drive shaft with a flange. The rotary shaft is first processed during manufacturing. Then the caster is matched with the conveyor belt to ensure the thick elastic rubber on the surface of the rotary shaft is matched. Through the driving wheel and the conveyor belt, the line contacts the flexible curved surface during movement, reducing rigid contact between the harvester parts and increasing overall harvester reliability. Due to the large span of the conveyor belt, four drive wheels are arranged symmetrically in pairs. The drive wheel is shown in Figure 5.

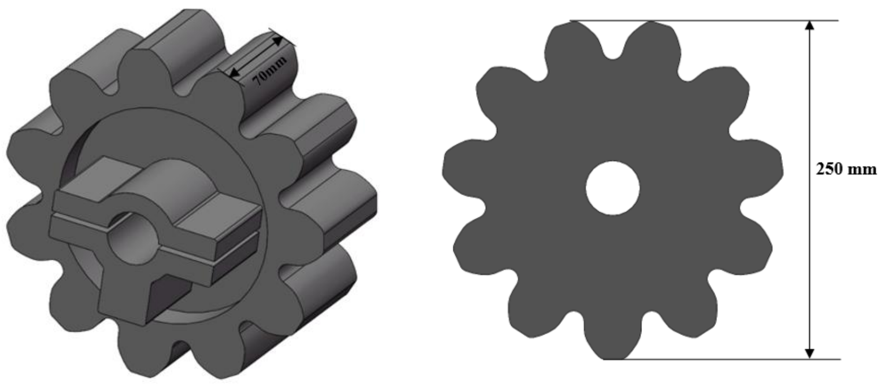

Fig. 5 - Drive wheel diagram

The separation conveyor speed is a key parameter of the separation conveyor device and is mainly controlled by the drive wheel. If the speed is too high, the vibration time of *Panax notoginseng* on the separation conveyor will be reduced, the rhizome-soil separation effect will be poor, the soil and impurities will not fall easily, and the excessive speed will also cause the tooth jump phenomenon; if the speed is too low, the soil will be piled up at the connection position between the excavation device and the separation conveyor device, reducing the harvesting efficiency. According to the supporting project's requirements, production efficiency should be ≥ 3 mu per hour. Combined with the operating width of the whole machine, it can be seen that the operating speed of the entire machine should be ≥ 0.38 $m \cdot s^{-1}$, so the speed of the separation conveyor should be greater than 0.38 $m \cdot s^{-1}$.

The drive wheel can be simplified as a polygonal rotating mechanism that drives the separation conveyor. By substituting the speed, number of teeth, and pitch into Eq. (1), the rotational speed *n* of the drive wheel can be obtained.

$$V_s = \frac{zpn}{60\times 1000} \tag{1}$$

where:

V_s is the separation conveyor speed [m·s-1]; p is the pitch of the drive wheel [mm]; n is the drive wheel speed [r·min-1]; z is the number of teeth of the drive wheel.

As shown in Figure 6, the velocity analysis of the separation conveyor indicates that the bar velocity can be decomposed into horizontal and vertical components.

$$\begin{cases} V_x = R\omega_1 cos\varphi' \\ V_y = R\omega_1 sin\varphi' \end{cases} \tag{2}$$

where:

R is the pitch radius of the drive wheel [mm]; ω_1 is the angular velocity of the drive wheel [rad·s-1]; φ' is the phase angle [°], i.e. the angle between the line connecting the center of the bar with the center of the drive wheel and the vertical center line.

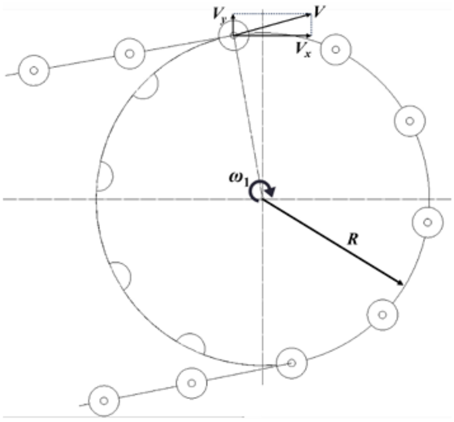

Fig. 6- Velocity analysis of the separation conveyor device

Based on the velocity analysis, the horizontal velocity component of the bar is responsible for conveying the material and therefore represents the conveying speed. Since the phase angle range is $-\frac{\pi}{2} \le \varphi \le \frac{\pi}{2}$, the following conclusions can be drawn.

$$\begin{cases} V_{\min} = R\omega_1 cos\frac{\pi}{2} = 0 \\ \varphi' = \pm\frac{\pi}{2} \end{cases} \tag{3}$$

When the phase angle is 90°, the separation conveyor bar and the drive wheel just come into contact and mesh, and the minimum lifting velocity is 0.

When the lifting velocity reaches its maximum value:

$$\begin{cases} V_{\max} = R\omega_1 \\ \varphi' = 0 \end{cases} \tag{4}$$

When the phase angle is 0, the bar coincides with the vertical centerline, and the velocity of the separation conveyor reaches its maximum value. At the next moment, the *Panax notoginseng* roots are thrown toward the lifting device. Therefore, to ensure smooth connection with the lifting-chain device, the radius and angular velocity of the drive wheel should be increased as much as possible. Accordingly, a drive wheel with 13 teeth, a diameter of 250 mm, and a width of 70 mm is selected and fixed to the drive shaft by means of a flange.

Determination of the vibration wheel

The vibration wheel is the main component of the separation conveyor device and the most critical component. The system realizes the rotation of the vibration wheel driven by the conveyor belt; the vibration wheel is an active double-roller vibration wheel (as shown in Figure 7). According to the overall configuration of the separation conveyor device and the transmission design requirements, the vibration wheel is installed between the front-driven wheel and the drive wheel. The upper part contacts the tight side of the conveyor belt. The single roller can rotate around its own fixed axis. The size is 70 mm in diameter and 75 mm in width. It is fixedly connected to the vibration shaft by a vibration wheel fixing plate.

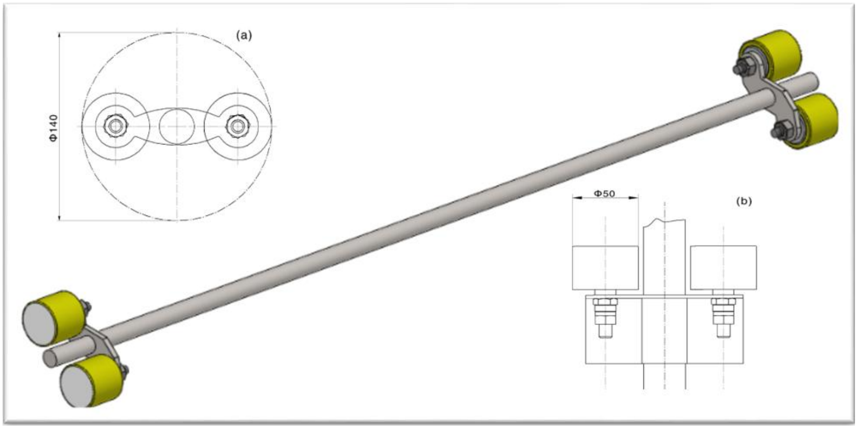

Fig. 7 - Structure diagram of the active vibration device

The active vibration device uses a hydraulic motor and is adjustable in speed. The vibration wheel shakes the separation conveyor twice for each rotation of the vibrating shaft. The vibration frequency is calculated as follows:

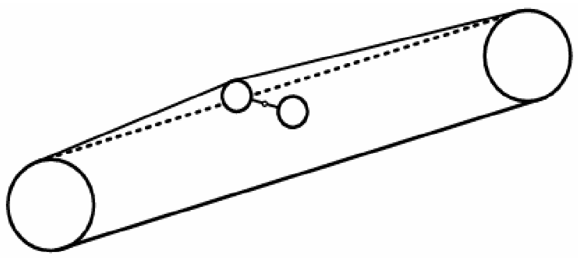

Fig. 8 - Vibration wheel working process diagram

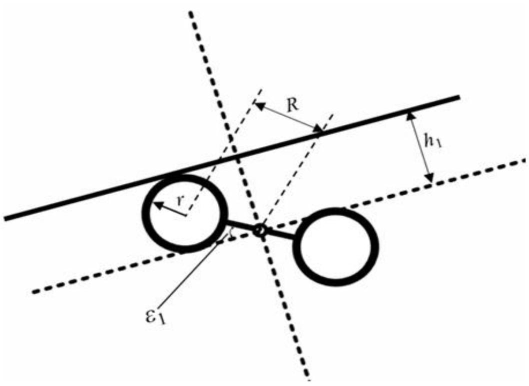

Fig. 9 - The vibration wheel lifts the separation conveyor

The calculation equation for the rotation angle of the vibration wheel is:

$$\varepsilon = \pm \arcsin\left(\frac{h_1 - r}{R}\right) + k\pi \tag{6}$$

where:

ε is the rotation angle of the vibration wheel [°]; h_1 is the distance between the vibration axis and the conveyor belt [mm]; *r* is the radius of the vibration wheel roller, [mm]; R is the distance from the origin to the center of the roller [mm]; k: natural number, k=0,1,2, …

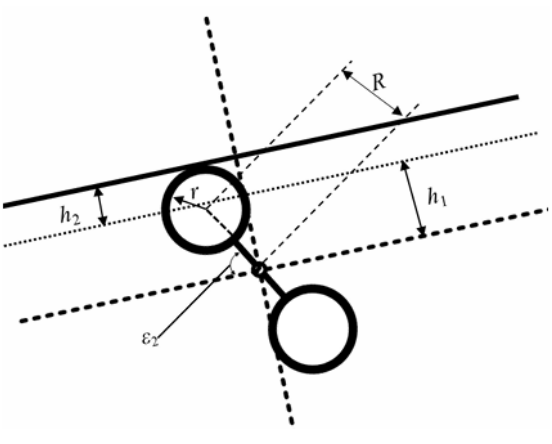

Fig. 10 - Schematic diagram of the conveyor belt lifted by the vibration wheel

As shown in Figure 10, when the vibration wheel lifts the conveyor belt, the contact point between the roller and the screen surface is displaced. The displacement can be divided into D_1 in the direction perpendicular to the conveyor belt and D_2 parallel to the conveyor belt. The displacement components are calculated using Eq. 7.

$$\begin{cases} D_1 = R|sin\varepsilon_2| + r - h_1 \\ D_2 = R|cos\varepsilon_1| - R|cos\varepsilon_1| \\ k\pi + \varepsilon_1 \geq \varepsilon_2 \geq (k+1)\pi - \varepsilon_1 \end{cases} \quad (7)$$

where:

ε_1 is the rotation angle before the vibration wheel lifts the screen surface [°]; ε_2 is the rotation angle after the vibration wheel lifts the screen surface [°].

The calculation equation for the rotation angle ε_2 after the vibration wheel lifts the screen surface is shown in equation 8.

$$\varepsilon_2 = \omega_2 t \quad (8)$$

where:

t is the rotation time of the vibration wheel (s).

Combining Eqs (7) and (8), the following equation can be obtained:

$$\begin{cases} D_1 = R|sin\omega_2 t| + r - h_1 \\ D_2 = R|cos\omega_2 t| - R|cos\varepsilon_1| \\ k\pi + \varepsilon_1 \geq \omega_2 t \geq (k+1)\pi - \varepsilon_1 \end{cases} \quad (9)$$

Taking the derivative of the above equation, the velocity of the screen contact point under the action of the vibration wheel can be obtained as follows:

$$\begin{cases} V_1 = \frac{Dd_1}{dt} = \omega_2 R\cos\omega_2 t \\ V_2 = \frac{Dd_2}{dt} = \omega_2 Rsin\omega_2 t \end{cases} \quad (10)$$

The acceleration of the screen contact point under the action of the vibration wheel can then be obtained as follows:

$$\begin{cases} a_1 = \frac{dV_1}{dt} = {\omega_2}^2 R\sin\omega_2 t \\ a_2 = \frac{dV_2}{dt} = {\omega_2}^2 R\cos\omega_2 t \end{cases} \quad (11)$$

Mechanical analysis of the separation conveyor device

The movement of the *Panax notoginseng* rhizome on the separation conveyor device can be roughly divided into four stages (*Wang et al., 2023a*): from the front guide wheel to the front end of the vibration wheel, the vibration wheel action stage, from the rear end of the vibration wheel to the end of the drive wheel, and from the end of the drive wheel to the lifting chain device. Since the movement of the *Panax notoginseng* rhizome from the front guide wheel to the end of the drive wheel is similar, only the two movement conditions on the separation conveyor device, and when thrown out from the end of the drive wheel are discussed and analyzed.

The *Panax notoginseng* rhizome is transported along the inclined surface on the separation conveyor device. When the screen surface is approximated as a straight line, and the air resistance is not considered, the force analysis of the *Panax notoginseng* rhizome is performed, as shown in Figure 11. To ensure the smooth transportation of the *Panax notoginseng* rhizome and the separation of the rhizome and soil, the following conditions should be met:

$$\begin{cases} f_s - \mathrm{mgsin}\alpha_s \geq \mathrm{ma_x} \\ F_N - \mathrm{mgcos}\alpha_s \geq \mathrm{ma_y} \end{cases} \quad (12)$$

where:

f_s is the friction between *Panax notoginseng* rhizome and screen surface, [N]; m is the mass of Panax notoginseng rhizome, [kg]; F_N is the support force of screen surface on *Panax notoginseng* rhizome, [N]; α_s is the angle between screen surface and horizontal plane, [N]; a_x: tangential acceleration of *Panax notoginseng* rhizome along screen surface, m·s^{-2}; a_y is the normal acceleration of *Panax notoginseng* rhizome along screen surface, m·s^{-2}.

To ensure that the rhizome of *Panax notoginseng* is hit by the vibration wheel and thrown up, the following conditions should be met:

$$\begin{cases} \frac{mg}{z}\omega_2{}^2(R+r)cos\alpha_s > mg \\ \omega_2 = \frac{nb}{30} \end{cases} \quad (13)$$

where:

n is the vibration wheel speed, [r·min^{-1}]; b is constant, [b=π^2].

Simplifying equation (13), the vibration wheel speed should satisfy:

$$n > 30\sqrt{\frac{1}{(R+r)cos\alpha_s}} \quad (14)$$

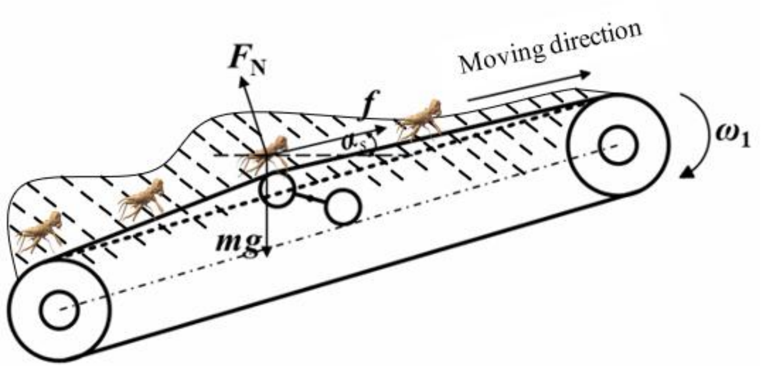

Fig. 11 - Mechanical analysis of the separation conveyor device

Analysis of the throwing motion at the end of the conveyor belt

After the rhizome of *Panax notoginseng* passes through the front end of the conveyor belt and the vibration wheel, it reaches the end and first does an oblique throwing motion, then a horizontal throwing motion, and finally goes to the lifting device. During the analysis, the screen surface is regarded as a plane, with the center of mass of the rhizome of *Panax notoginseng* as the origin, the horizontal right is the positive direction of the X-axis, and the vertical upward is the positive direction of the Y-axis. Without considering the air resistance, the displacement and velocity of the rhizome of *Panax notoginseng* are analyzed, as shown in Figure 12. Assume that the initial velocity of the rhizome of *Panax notoginseng* is v_a, which can be decomposed into the velocity vax in the X-axis direction and the velocity v_{ay} in the Y-axis direction, and satisfies the following relationship:

$$\begin{cases} v_{ax} = v_a cos\theta_s \\ v_{ay} = v_a sin\theta_s \end{cases} \quad (15)$$

where: θ_s: screen surface inclination [°]; v_{ax}: X-axis speed [m·s^{-1}]; v_{ay}: Y-axis speed [m·s^{-1}].

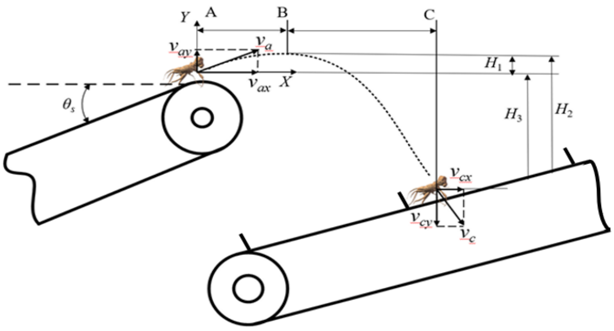

Fig. 12 - Throwing-motion analysis of *Panax notoginseng* rhizomes

The rhizome of *Panax notoginseng* performs oblique projectile motion in the AB section and horizontal projectile motion in the BC section. The displacement and velocity analyses of the two sections have been performed. The displacement analysis of the oblique projectile motion in the AB section is shown in equations (16), (17), and (18) since point B is the end point of the oblique projectile motion of the rhizome of *Panax notoginseng*, the vertical velocity v_{by} = 0 and the horizontal velocity v_{bx} = cosθ of the rhizome of *Panax notoginseng* at point B.

$$H_1 = \frac{v_{ay}{}^2}{2g} \quad (16)$$

$$X_1 = v_{ax} t_1 \tag{17}$$

$$t_1 = \frac{v_{ay}}{g} \tag{18}$$

where:

H_1 is the vertical displacement of segment AB, [m]; X_1 is the horizontal displacement of segment AB, [m]; t_1 is the time taken for segment AB, [s]; g is the gravitational acceleration, [m·s^{-2}], g=9.8 m·s^{-2}.

The displacement analysis of the BC segment horizontal projection motion is shown in equations (19), (20), and (21):

$$H_2 = H_1 + H_3 \tag{19}$$

$$X_2 = v_{ax} t_2 \tag{20}$$

$$t_2 = \sqrt{\frac{2H_2}{g}} \tag{21}$$

where:

H_2 is the vertical displacement of BC segment, [m]; H_3 is the drop height of *Panax notoginseng* rhizome from the end of the separation conveyor to the lifting chain device, [m]; t_2 is the time taken for BC process, [s]. By combining and simplifying Eqs. (16)–(21), the displacement and time required for the *Panax notoginseng* rhizomes to be thrown from the end of the separation conveyor to the lifting-chain device can be obtained, as shown in the following equations:

$$H_2 = \frac{{v_{ay}}^2}{2g} + H_3 \tag{22}$$

$$t = \frac{v_{ay}}{g} + \sqrt{\frac{2\left(\frac{{v_{ay}}^2}{2g} + H_3\right)}{g}} \tag{23}$$

$$t = v_{ax}\left(\frac{v_{ay}}{g} + \sqrt{\frac{2\left(\frac{{v_{ay}}^2}{2g} + H_3\right)}{g}}\right) \tag{24}$$

Since point C is the end point of the horizontal motion, the horizontal velocity of point C $v_{cx}= v_a\cos\theta$, and the vertical velocity and the resultant velocity are shown in the following equation.

$$v_{cy} = g t_2 = \sqrt{{v_{ay}}^2 + 2gH_3} \tag{25}$$

$$v_c = \sqrt{{v_{cx}}^2 + {v_{cy}}^2} = \sqrt{(v_a cos\theta)^2 + {v_{ay}}^2 + 2gH_3} \tag{26}$$

In summary, the speed and displacement of *Panax notoginseng* rhizome from the end of the separation conveyor to the lifting device are primarily determined by the initial speed, screen surface inclination, and drop height. To ensure that the *Panax notoginseng* rhizomes can fall smoothly from the separation conveyor to the lifting device, the initial speed and drop height should be increased as much as possible, and the screen surface angle should be reduced. The conveying speed is taken as 0.6~1.4 m·s^{-1}, and the inclination angle is 15~35°.

Simulation analysis and test of the separation conveyor device

Establishing the separation conveyor simulation environment

Soil particle size and distribution data were measured, and the soil discrete element particle model was divided into three categories. The default spherical particles in EDEM were used. The soil particle shape, size, and proportions are shown in Table 2 and were added as the second category of bulk particles.

In RecurDyn, create a Wall file from the completed multibody dynamics model. Enable the RecurDyn-EDEM coupling interface and import the metal model's Wall file into EDEM's Geometry window, as shown in Figure 13. Create a solid thin plate at the bottom and end of the lifting chain to simulate the soil drop and the transition between the *Panax notoginseng* rhizome-soil complex and the next-level working component. Set the physical properties of the *Panax notoginseng* rhizome, soil particles, and metal model, enter the contact parameters, select the JKR contact model, and set the surface energy parameters for the contact.

Table 2

Soil discrete element particle model

Name	Model	Diameter / mm	Scale / %
Single spherical particles	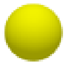	1.6	33.9
Double-spherical particles	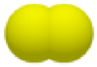	3.6	25.2
Triple-spherical particles	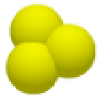	5.2	41.3

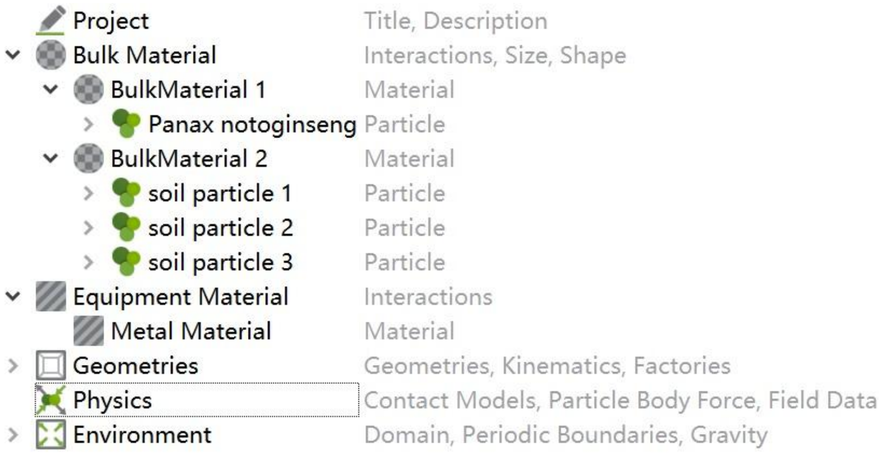

Fig. 13 - Establishment of granular and metallic materials

A virtual cube with an edge length of 0.2 m is generated at the front of the elevator chain. The Y-direction is defined as the gravity direction, and the acceleration is 0.98 m·s^{-2}, as shown in Figure 14.

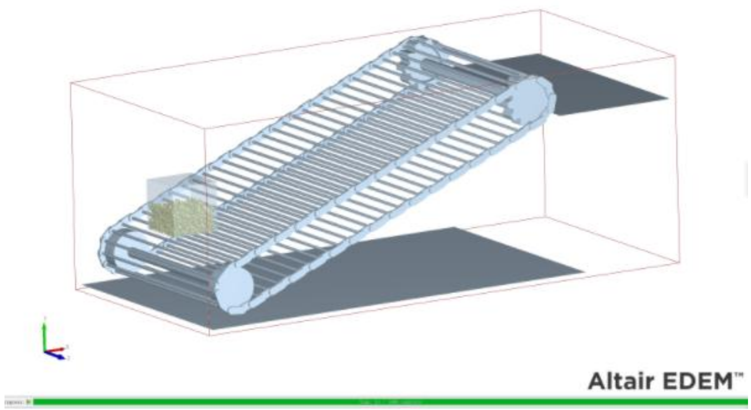

Fig. 14 - Establishment of coupled simulation environment

A discrete element model of the *Panax notoginseng* rhizome stem is generated within the box, enclosing a predetermined proportion of soil particles. This simulates the actual production process of the *Panax notoginseng* rhizome-soil complex as it is transported and separated by the elevator chain. At this point, the simulation environment is set up, and the coupled simulation can begin. Set the simulation time to 4 s and the step size to 0.01 s.

Simulation test results of the separation conveyor device

Overall movement of the *Panax notoginseng* rhizome-soil complex

The simulation results show that the rhizome-soil separation of the *Panax notoginseng* rhizome-soil complex was essentially complete within 2.25 seconds of simulation. Therefore, the main focus was on observing the conveying and separation movement characteristics of the *Panax Notoginseng* rhizome-soil complex during the period 0 to 2.2 seconds. The lifting velocity was 0.8 m·s^{-1} and the lifting angle was 25°, as shown in Figure 15.

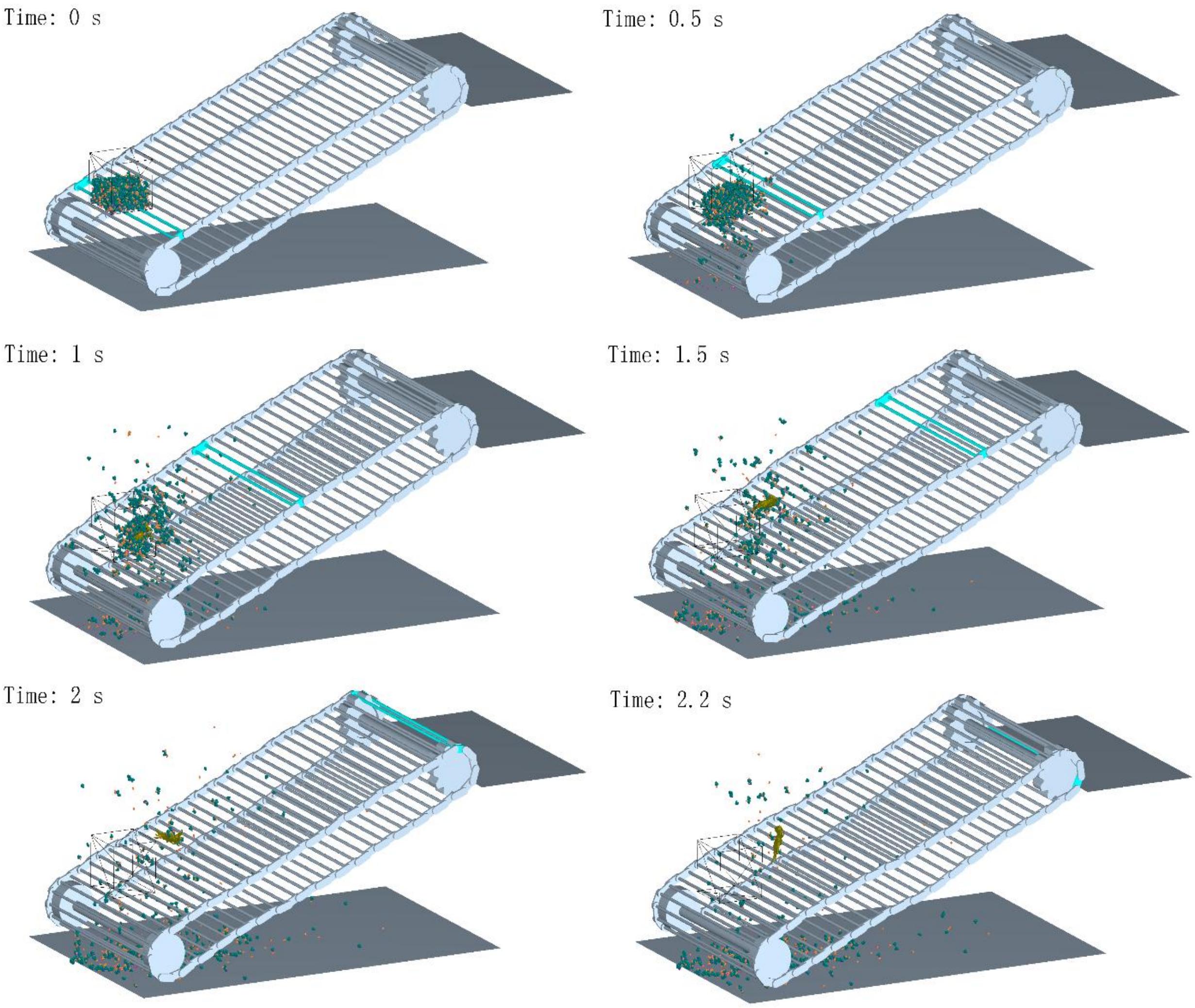

Fig. 15 - Movement trajectory of the *Panax notoginseng* rhizome-soil composite

To observe the relative motion of the *Panax notoginseng* rhizome soil complex and the lifting chain, use the blue bar below the virtual box as the observation point. The *Panax notoginseng* rhizome-soil complex freely falls onto the screen surface. Some loose, fine soil particles escape directly through the gaps between the bars, while the majority of the soil adheres to the surface of the *Panax notoginseng*. The relative friction between the *Panax notoginseng* rhizome-soil complex and the screen surface tends to transport the material diagonally upward. The vibration of the elevator chain gradually separates the *Panax notoginseng* roots from the soil particles, and the separation efficiency gradually increases as the amount of soil in the *Panax notoginseng* rhizome-soil complex decreases. Due to the low gravity, the soil particles are struck by the bars and scattered, resulting in significant variations in their velocities. However, the velocity of the *Panax notoginseng* rhizome on the screen surface does not change significantly, and the conveying speed is lower than the lifting speed. In EDEM post-processing, the *Panax notoginseng* particles were set to Steam mode. The *Panax notoginseng* rhizome exhibits "bouncing" and "backflowing" on the elevator chain. The degree of "bouncing" and "backflowing" becomes more pronounced as the number of soil particles attached to the rhizome decreases.

Rhizome-soil separation of Panax notoginseng rhizome-soil complex

To observe the effect of rhizome-soil separation in the coupled simulation of the *Panax notoginseng* rhizome-soil complex, the 3D Viewer-Setup Selections-Grid Bin Group function in the EDEM post-processing module was used to partition the particle computational domain. Three soil particle groups were selected for computational particle grouping. The dimensions and position of the Gind Bin Group were set, along with the number of bins. The computational domain was rotated along the Z-axis to an angle parallel to the elevator chain screen surface. Using a 0.4s time frame as an example, the soil particle computational domain partitioning is shown in Figure 16.

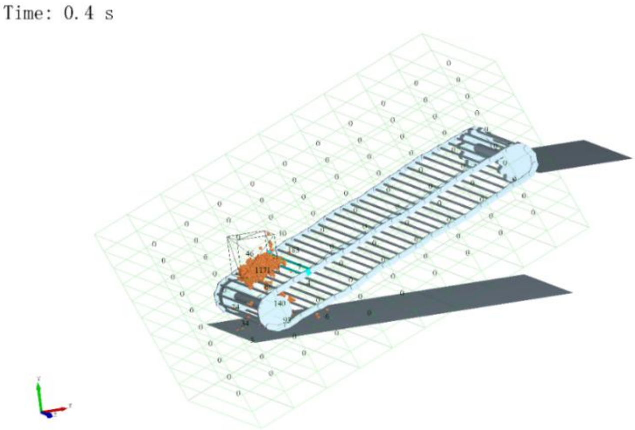

Fig. 16 - Gind Bin Group setting

The separation of the rhizome and soil in the *Panax notoginseng* rhizome-soil complex is expressed as the sieving rate. There are 1,800 soil particles of varying sizes and shapes. By counting the number of particles attached to the *Panax notoginseng* at each step, the sieving rate of the *Panax notoginseng* rhizome-soil complex can be calculated. The calculation equation is as follows:

$$Z_s = \frac{n_s}{N_s} \times 100\% \tag{27}$$

where: Z_s is the Simulated sieving efficiency of the *Panax notoginseng* root-soil complex, [%]; n_s is the Number of soil particles attached to the *Panax notoginseng*; T_s is the Total number of soil particles.

The sieving rate of the *Panax notoginseng* rhizome-soil composite was calculated for each step length, ranging from 0 to 2.20 seconds. The trajectory of soil particle motion is plotted in Figure 17. The sieving rate curve is plotted in Figure 18. Single spherical particles are purple, double spherical particles are orange, and triple spherical particles are green. The sieve clearance rate of the *Panax notoginseng* rhizome-soil complex increased rapidly within 0.25 s, then slowly increased until it approached 100%. This is because finely divided single-spherical particles separated preferentially; double-spherical particles separated in the middle section; and triple-spherical particles had strong adhesion to the *Panax notoginseng* rhizome, bouncing on the sieve surface with the *Panax notoginseng* and gradually separating.

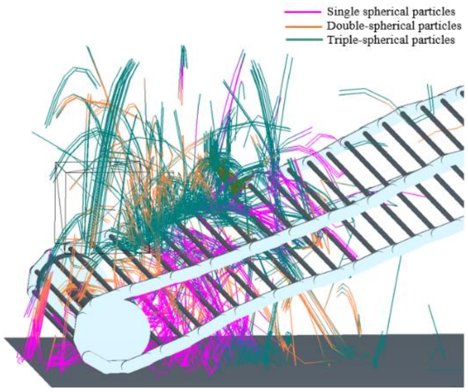

Fig. 17 - Soil particle motion trajectory

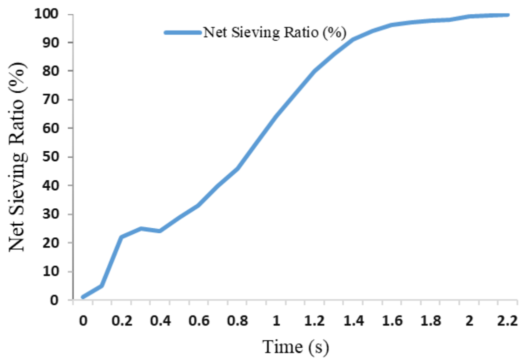

Fig. 18 - Sieve clearance rate curve

Dynamic analysis of Panax notoginseng rhizome

To investigate the motion and forces acting on *Panax notoginseng* rhizome on the separation conveyor, a triaxial force curve for *Panax Notoginseng* particles was plotted, as shown in Figure 19. At the front end of the separation conveyor, the *Panax Notoginseng* rhizome-soil complex exhibits high soil adhesion and is relatively heavy, making it difficult to lift. Therefore, from 0 to 0.75 s, the forces acting on the *Panax Notoginseng* rhizome are uneven and exhibit irregular variations. After 0.75 s, the forces acting on the *Panax Notoginseng* rhizome fluctuate dramatically at regular intervals, primarily due to the vibration of the separation conveyor. The moment the rod strikes the rhizome, the forces acting on the rhizome vary significantly. The *Panax notoginseng* rhizome is mainly subjected to the force in the X-axis and Y-axis directions on the inclined plane of the separation conveyor.

The friction between the *Panax notoginseng* rhizome-soil composite and the separation conveyor mainly provides the force on the X-axis. At the moment when the rod hits the *Panax notoginseng* rhizome, the *Panax notoginseng* rhizome is mainly subjected to the force in the normal direction of the separation conveyor, which is manifested as the force in the positive direction of the Y-axis and the force in the negative direction of the X-axis. After being thrown up, the force received by the *Panax notoginseng* is the gravity in the negative direction of the Y-axis, and the forces on the X-axis and Z-axis are close to zero.

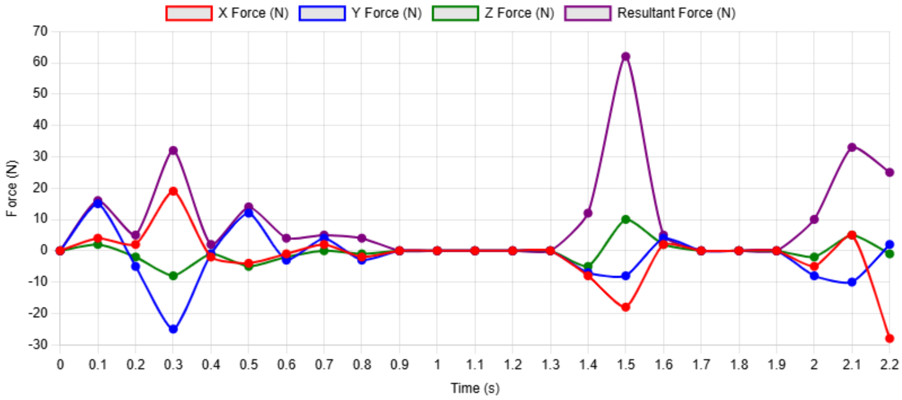

Fig. 19 - Force variation curve of Panax notoginseng rhizome

The forces acting on the three axes of the *Panax notoginseng* rhizome drive the changes in its velocity along these three axes, as shown in Figure 20. The velocity on the Z axis changes slightly, at around 0 m·s^{-1}, indicating that the movement of the *Panax notoginseng* rhizome in the axial direction of the rod is not apparent; the velocity on the X axis is positive within 0-1.7 s, indicating that the *Panax notoginseng* lifting effect is significant; the velocity on the X axis is negative within 1.7-2.2 s, indicating that the movement direction of the *Panax notoginseng* rhizome is rolling downward along the separation conveyor, with "backflow" occurring; the velocity on the Y axis fluctuates regularly in the positive and negative directions, indicating that the *Panax notoginseng* rhizome vibrates significantly on the separation conveyor, and the greater the fluctuation amplitude, the greater the height to which the Panax notoginseng is thrown.

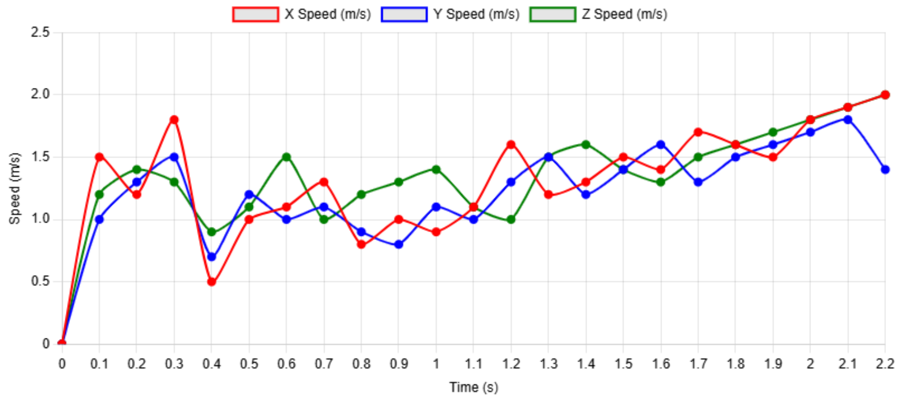

Fig. 20 - Speed variation curve of *Panax notoginseng* rhizome

Lab Test of the separation conveyor

To assess the performance of the separation conveyor device in the *Panax notoginseng* harvester, a bench test was conducted at the Research Center on Mechanization Engineering of Chinese Medicinal Materials in Yunnan. The lab test utilized a separation conveyor device capable of adjusting multiple operational parameters. The drive shaft's height, which influences the lifting angle, is adjustable via a two-link worm-gear lift, while vibration amplitude is controlled by varying the distance between the vibration shaft and the working surface. An inverter controls the conveyor's speed and vibration frequency by driving two three-phase asynchronous motors. The frame comprises a 6 mm-thick Q235 steel plate and a galvanized square tube, with adjustment mechanisms for inclination angle and vibration amplitude, facilitated by a drive shaft and laser-cut sliding grooves. Asynchronous motors power two turbine screw lifters synchronously to maintain the setup's stability. The primary *Panax notoginseng* harvester separation conveyor device is shown in Figure 21.

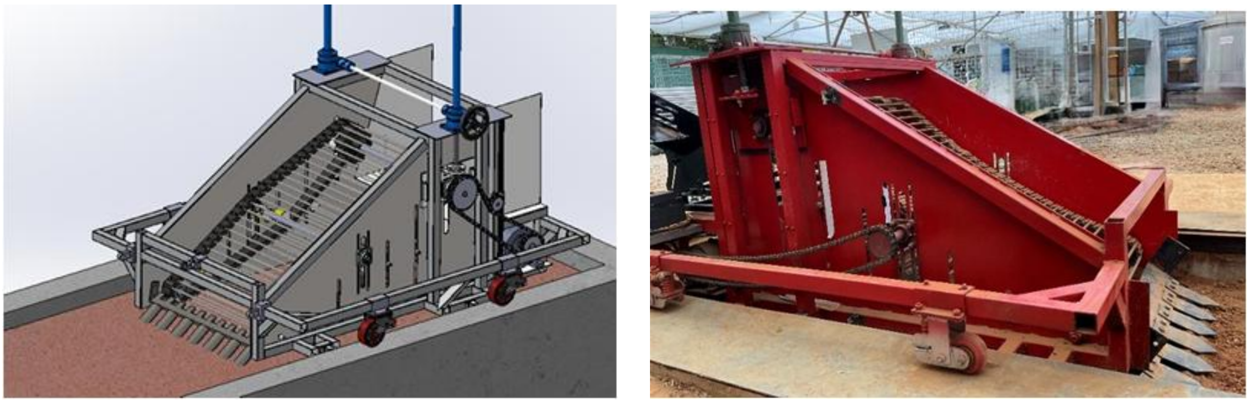

Fig. 21 - The separation conveyor device lab test prototype

Test plan and evaluation indicators

According to theoretical calculations and operational requirements, the main factors affecting the performance of the separation conveyor device are conveyor speed, conveyor inclination angle, and vibration frequency. Referring to the design and analysis of key component parameters, it is known that the conveyor inclination is changed by adjusting the platform separation conveyor device, and the preset range is 15°~35°; the YVR-1 digital tachometer of Yatai Optoelectronics is used to measure the conveying shaft speed of the two three-phase asynchronous motors under no-load conditions (Figure 22). The conveyor drive wheel ratio converts the drive wheel and vibration wheel speeds, and then the conveyor speed and vibration frequency are calculated. The preset conveyor speed is 0.6~1.4 m·s⁻¹, and the preset vibration frequency is 1~3 Hz.

Fig. 22 - Rotational speed measurement

Experiments were conducted to determine the optimal operating parameters of the separation conveyor device, using the separation and conveying rates as evaluation criteria. The conveying rate Y_1 refers to the ratio of the number of *Panax notoginseng* transported by the separation conveyor to the next stage of working components within a specific period to the number of *Panax notoginseng* entering the separation conveyor, and the calculation equation is:

$$Y_1 = \frac{N}{M} \times 100\% \tag{28}$$

where: Y_1 is the conveying rate, [%]; N is the number of particles passing through the separation conveyor; M is the number of particles entering the separation conveyor.

The separation rate Y_2 is the percentage of the actual mass of the separated material to the mass of the material that should be separated. The mass of soil and other impurities separated by the separation conveyor device per unit time, and the mass of impurities attached to the rhizome of *Panax notoginseng* after separation, are measured to facilitate detection of the separation process. The separating rate calculation equation is:

$$Y_2 = \frac{m_1}{m_1 + m_2 - m_3} \times 100\% \tag{29}$$

where: Y_2 is the separation rate, [%]; m_1 is the mass of impurities separated after separating, [g]; m_2 is the mass of *Panax notoginseng* rhizome and soil after separating, [g]; m_3 is the mass of *Panax notoginseng* rhizome, [g].

Orthogonal test design

To explore the influence of each experimental factor and its interaction on the quality of conveying and separation operation, the lifting speed X_1 is 0.6, 0.8, and 1.0 m·s^{-1}, the vibration frequency X_2 is 1 Hz, 1.5 Hz, and 2 Hz, and the lifting angle X_3 is selected as 15°, 20°, and 25°. The conveying and separating rates are used as experimental indicators in the orthogonal rotation combination test for quadratic regression (Figure 23). The level coding of the experimental factors is shown in Table 3.

Fig. 23 - Separation conveyor device lab test

Table 3

Experimental factors and codes

Code	Experimental factor Lifting speed X_1/m·s^{-1}	Vibration frequency X_2/Hz	Lifting angle X_3 /°
1.682	1.14	2.34	28.40
1	1.0	2.0	25
0	8.0	1.5	20
-1	0.6	1.0	15
-1.682	0.46	0.66	11.60

Orthogonal Experimental results

The Experimental plan and results are shown in Table 4. A total of 23 test groups were conducted, and the test was repeated 3 times at each combination level. The arithmetic mean was taken as the test value of the conveying and separating rates.

Table 4

Experimental plan and results

Serial Number	Factor			Conveying rate	Separation rate
	X_1	X_2	X_3	Y_1/%	Y_2/%
1	-1	-1	-1	92.45	90.78
2	1	-1	-1	91.63	92.02
3	-1	1	-1	82.96	92.47
4	1	1	-1	88.69	91.21
5	-1	-1	1	92.47	90.18
6	1	-1	1	94.33	91.62
7	-1	1	1	87.58	93.07
8	1	1	1	96.85	93.31
9	-1.682	0	0	82.36	90.29
10	1.682	0	0	90.72	93.00
11	0	-1.682	0	94.74	90.89
12	0	1.682	0	90.14	93.94
13	0	0	-1.682	92.15	92.57
14	0	0	1.682	92.84	94.11
15	0	0	0	95.63	93.92
16	0	0	0	95.74	94.44

Serial Number	Factor			Conveying rate	Separation rate
	X_1	X_2	X_3	Y_1/%	Y_2/%
17	0	0	0	94.97	94.36
18	0	0	0	96.04	93.98
19	0	0	0	95.47	94.25
20	0	0	0	96.16	94.23
21	0	0	0	94.89	94.08
22	0	0	0	95.72	94.35
23	0	0	0	95.36	94.00

$$Y_1 = 95.53866 + 2.20391X_1 - 1.65008X_2 + 1.21982X_3 + 1.74500X_1X_2 + 0.777500X_1X_3 + 1.25750X_2X_3 - 3.04412{X_1}^2 - 0.958665{X_2}^2 - 0.939224{X_3}^2 \tag{30}$$

$$Y_2 = 94.19028 + 0.455272X_1 + 0.775363X_2 - 0.314116X_3 - 0.462500X_1X_2 + 0.212500X_1X_3 + 0.462500X_2X_3 - 1.00566{X_1}^2 - 0.733492{X_2}^2 - 0.406535{X_3}^2 \tag{31}$$

Design-Expert 13 software was used to analyze the conveying and separation rates test results using variance ANOVA. The significance test results are shown in Table 5. The results in the table show that the experimental model is highly statistically significant ($p < 0.0001$), indicating that the designed test is reasonable and practical. The determination coefficient R^2 for Y_1 and Y_2 are 0.9589 and 0.9360, respectively, implying that the regression equation has a high degree of fitting; in summary, the models can be used for analysis and optimization. The experimental factors lifting speed X_1, vibration frequency X_2, and lifting angle X_3 all significantly affect the conveying rate Y_1 and the separation rate Y_2 ($p < 0.05$). The interaction term between lifting speed and vibration frequency (X_1 X_2), as well as the vibration frequency and lifting angle (X_2 X_3), has a significant influence on the conveying Y_1 and separation Y_2 rates ($p < 0.05$), the interaction term between lifting speed and lifting angle (X_1 X_3) had a non-significant effect on the conveying Y_1 and separation Y_2 rates ($P>0.05$). The squared terms X_1^2, X_2^2, and X_3^2 significantly affected the Y_1 and Y_2 ($p < 0.01$).

Table 5

Variance analysis

Source of variation	Conveying rate					Separation rate				
	Sum of squares	Freedom	Mean square	*F*	*P*	Sum of squares	Freedom	Mean square	*F*	*P*
Model	340.17	9	37.80	33.73	< 0.0001***	43.11	9	4.79	21.11	< 0.0001***
X_1	66.34	1	66.34	59.20	< 0.0001***	2.83	1	2.83	12.48	0.0037***
X_2	37.19	1	37.19	33.18	< 0.0001***	8.21	1	8.21	36.19	< 0.0001***
X_3	20.32	1	20.32	18.13	0.0009***	1.35	1	1.35	5.94	0.0299**
X_1X_2	24.36	1	24.36	21.74	0.0004***	1.71	1	1.71	7.54	0.0167**
X_1X_3	4.84	1	4.84	4.32	0.0582*	0.3613	1	0.3613	1.59	0.2292
X_2X_3	12.65	1	12.65	11.29	0.0051***	1.71	1	1.71	7.54	0.0167**
X_1^2	147.30	1	147.30	131.44	< 0.0001***	16.08	1	16.08	70.86	< 0.0001***
X_2^2	14.61	1	14.61	13.04	0.0032***	8.55	1	8.55	37.69	< 0.0001***
X_3^2	14.02	1	14.02	12.51	0.0036***	2.63	1	2.63	11.58	0.0047***
Residual	14.57	13	1.12			2.95	13	0.2269		
Lack of fit	13.07	5	2.61	13.96	0.0009***	2.66	5	0.5326	14.88	0.0007***
Error	1.50	8	0.1872			0.2863	8	0.0358		
Sum	354.73	22				46.06	22			

Note: * indicates significant impact (0.05<P<0.1), * * indicates significant impact (0.01<P<0.05), and * * * indicates extremely significant impact (P<0.01).

The *Panax Notoginseng* rhizome conveying rate constantly changes during operation, and the average value during the period of constant speed stability is the *Panax notoginseng* rhizome conveying rate. The changes in the conveying rate obtained are shown in Figure 24. Response surface plots were generated using Design-Expert 13 to visualize the effects of the factors above on the conveying rate. Figure 24a shows that the *Panax notoginseng* rhizome conveying rate Y_1 decreases slightly with increased vibration frequency X_2. With the increase in lifting speed X_1, the conveying rate Y_1 first increases and then decreases. Figure 24b shows that the conveying rate Y_1 increases with the lifting angle X_3, first and then decreases, as the ratio of lifting speed X_1 to lifting angle X_3 increases. Figure 24c shows that the conveying rate Y_1 decreases significantly with the increase in vibration frequency X_2, and the conveying rate Y_1 is not considerably affected by the lifting angle X_3 ratio to vibration frequency X_2.

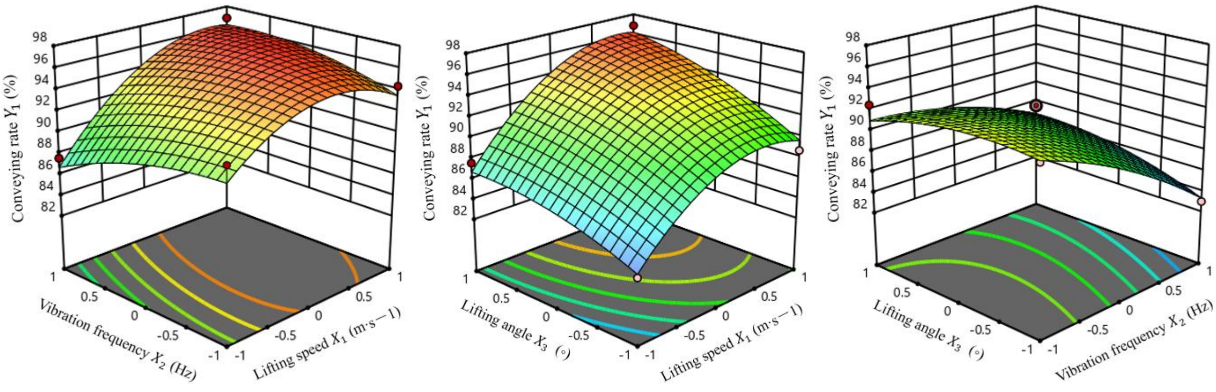

(a) (b) (c)

Fig. 24 - Response surface of interaction factors to the *Panax Notoginseng* rhizome conveying rate Y_1
(a) response surface under factors X_1 and X_2; (b) response surface under factors X_1 and X_3; and (c) response surface under factors X_2 and X_3

Figure 25 indicates the *Panax notoginseng* rhizome separation rate Y_2. Figure 25d shows that the separation rate Y_2 increases with an increasing lifting speed X_1 and vibration frequency X_2 from -1 to 1. Figure 25e shows that the conveying rate Y_2 increases slightly with increasing lifting speed X_1 and lifting angle X_3, and first increases and then decreases as X_1 increases from 0 to 1. The rhizome separation rate Y_2 gradually increases as the vibration frequency X_2 from -1 to 1 increases, and the separation rate Y_2 is not considerably affected by the lifting angle X_3 ratio to vibration frequency X_2, as shown in Figure 25f.

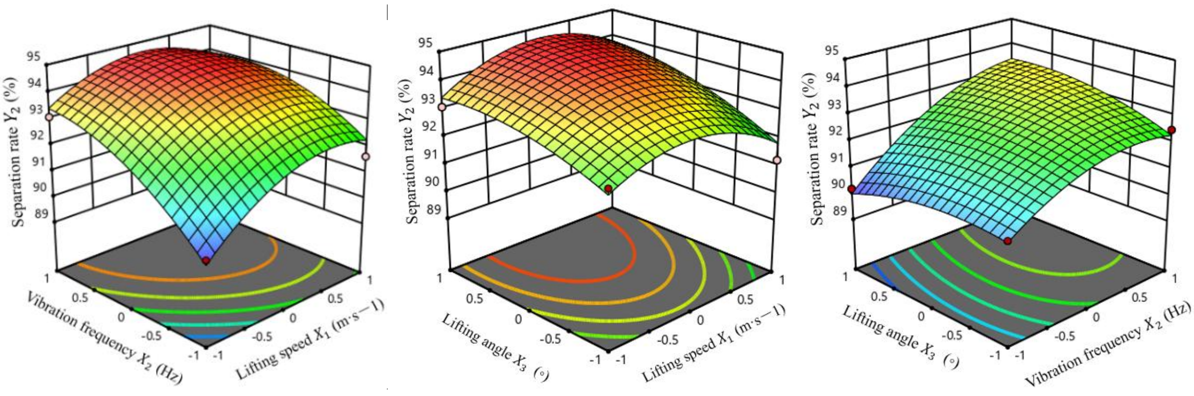

(d) (e) (f)

Fig. 25 - Response surface of interaction factors to the *Panax Notoginseng* rhizome separation rate Y_2
(d) response surface under factors X_1 and X_2; (e) response surface under factors X_1 and X_3; and (f) response surface under factors X_2 and X_3

Field validation experiment

Experimental design

The machining and assembly of the whole machine were completed based on the structural parameters of the separation conveyor device. Field validation tests were conducted in November 2025 at the *Panax notoginseng* farm in Shilin County, Kunming City, Yunnan Province, to evaluate the practical applicability and reliability of the device under real-world agricultural conditions. The operation parameters of the separation conveyor device during the field harvesting experiment are shown in Table 6.

Figure 26 depicts the scenario for field harvesting operations. Test tools include a steel tape measure, an electronic stopwatch, an electronic balance, a temperature and humidity meter, a soil moisture tester, and a digital display soil hardness meter. The experiment design of the field during the harvest period of *Panax Notoginseng* is as follows: the average ridge width of *Panax Notoginseng* is 1400 mm, the average ridge height is 200 mm, the average thickness of the mixture of *Panax Notoginseng* and soil is 100-150 mm, and the average diameter of rhizome is 26.3 mm, soil moisture content 13.2%, the soil is soft and sticky, with moderate cohesion. The weather is sunny, and the average temperature at harvest is 24°, with a relative humidity of 71%.

Table 6

Operation parameters of the separation conveyor device

Parameter	Numerical value
Working inclination angle of separation conveyor (◦)	20
Working speed of separation conveyor ($m \cdot s^{-1}$)	0.8
Vibration frequency (Hz)	1.5

Fig. 26 - Field harvesting experiment

Test measurements

(1) *Panax Notoginseng* conveying rate:

The *Panax Notoginseng* conveying rate (T) was calculated to determine how the mass of the *Panax Notoginseng* remained unconveyed. It was defined as follows:

$$T = \frac{W_1}{W_1 + W_2} \times 100\% \tag{32}$$

where W_1 is the total mass of harvested Panax Notoginseng (kg), and W_2 is the total mass of unharvested *Panax Notoginseng* (kg).

(2) *Panax Notoginseng* damage rate:

After *Panax Notoginseng* was harvested by machine, the harvested rhizomes were categorized into two groups: reasonable and damaged. The weight of each rhizome group was measured individually. The total damage rate (D) of the *Panax notoginseng* can be gained from the following equation:

$$D = \frac{W_4}{W_3 + W_4} \times 100\% \tag{33}$$

where W_3 is the total mass of good *Panax Notoginseng* (kg); W_4 is the mass of damaged *Panax Notoginseng* by the harvester machine (kg).

(3) Separation rate:

$$S = \frac{m_1}{m_1 + m_2 - m_3} \times 100\% \tag{34}$$

where S is the separation rate, %; m_1 is the mass of impurities separated after separating, (kg); m_2 is mass of *Panax notoginseng* rhizome and soil after separating, (kg); m_3 is the mass of *Panax notoginseng* rhizome, (kg).

Field experiment results

The treatments were randomly distributed in the main subplot and sub-subplot; the sub-subplot area was 52.5 m² (35×1.5 m), with 1.5 m between sub-subplots and 10 m at the end of each sub-subplot. After each subplot of experiments is completed, the data collection is carried out within half an hour to ensure consistent rhizome moisture evaporation. The average value is then calculated using the test data from the sub-subplots. The average value of all measured data is used as the final evaluation indicator. The results of the field test are listed in Table 7.

Table 7

Experimental results

Serial Number	Separation rate/%	Conveying rate/%	Damage rate/%
1	96.45	95.25	2.07
2	97.16	95.44	1.86
3	96.38	96.85	2.18
4	96.67	97.13	1.55
5	97.11	96.71	1.93
6	95.92	96.83	1.28
7	97.23	97.14	2.05
8	98.06	95.94	2.13
Average	96.87	96.42	1.88

DISCUSSION

The average values for the efficiency of *Panax notoginseng*-soil separation, the conveying rate of *Panax notoginseng*, and the rhizome damage rate for the separation conveyor device are 96.87%, 96.42%, and 1.88%, respectively. The relative errors between the laboratory and field test results for the efficiency of *Panax notoginseng*-soil separation and the rhizome conveying rate are 0.97% and 1%, respectively. These values are consistent with the optimized parameters and meet the agronomic requirements for *Panax notoginseng* harvesting. The separation rate of *Panax notoginseng* increased by 0.10%, and the damage rate decreased by 0.99% compared to the reference (*Zhenmeng et al., 2018*). The results indicate that the separation conveyor device yields a higher harvest of *Panax notoginseng* in hilly areas.

CONCLUSIONS

(1) This study systematically investigated the design, analysis, and optimization of a separation conveyor device for a self-propelled *Panax notoginseng* combine harvester, addressing the challenges of harvesting in hilly and mountainous regions of southwest China. By integrating agronomic characteristics of *Panax notoginseng* with mechanical design principles, a crawler-type harvester capable of excavation, separation, conveying, lifting, and collection was successfully developed to improve harvesting efficiency and reduce labor intensity.

(2) Through detailed kinematic and mechanical analyses, the separation conveyor structure and key components such as the drive wheel, vibration wheel, and bar-type conveyor were theoretically modeled and optimized. Coupled DEM–MBD simulations using EDEM and RecurDyn provided insights into soil–rhizome interaction, particle separation behavior, and dynamic forces acting on *Panax notoginseng* rhizomes. Simulation results demonstrated that effective soil separation could be achieved within approximately 2.25 s, with finer soil particles separating earlier than larger aggregates.

(3) Laboratory experiments and quadratic regression orthogonal tests further validated the simulation outcomes. Conveyor speed, vibration frequency, and lifting angle were identified as significant factors influencing conveying and separation performance. Optimal parameters were determined as a conveyor speed of 0.8 $m \cdot s^{-1}$, vibration frequency of 1.5 Hz, and lifting angle of 20°, achieving separation and conveying rates exceeding 95% under laboratory conditions.

(4) Field validation experiments confirmed the reliability and applicability of the optimized design. The separation conveyor achieved an average separation rate of 96.87%, conveying rate of 96.42%, and a low rhizome damage rate of 1.88%, meeting agronomic and mechanization requirements. Overall, this research provides a solid theoretical and experimental foundation for advancing mechanized harvesting of *Panax notoginseng* and similar rhizome crops.

ACKNOWLEDGEMENT

We would like to express our sincere appreciation to all those who supported and contributed to this research. Special thanks to the Research Center on Mechanization Engineering of Chinese Medicinal Materials in Yunnan Universities for providing invaluable resources and support throughout this study, under project number 2022YFD2002004. We also extend our gratitude to the Faculty of Mechanical and Electrical Engineering and Faculty of Modern Agricultural Engineering, Kunming University of Science and Technology, Kunming, China, for their collaboration and valuable contributions, Additionally, we acknowledge the School of Tea and Coffee, Puer University, Puer, China. and the Agricultural Engineering Research Institute (AEnRI), Agricultural Research Center (ARC), 256 Dokki, Giza, Egypt.

REFERENCES

[1] Chen, M., Liu, X., Hu, P., Zhai, X., Han, Z., Shi, Y., Zhu, W., Wang, D., He, X., Shang, S., (2024), Study on rotor vibration potato-soil separation device for potato harvester using DEM-MBD coupling simulation, *Computers and Electronics in Agriculture* Vol. 218, https://doi.org/10.1016/j.compag.2024.108638.

[2] Cheng, Z., Yang, D., Wang, X., Liu, M., Li, Y., Chen, X., (2023), Development Status and Prospect of Potato Mechanized Harvest in Hilly and Mountainous Areas, *AGRICULTURAL ENGINEERING* Vol. 13, no.11, pp. 5-12, DOI：10.19998/j.cnki.2095-1795.2023.11.001.

[3] Faan, W., Chang, N., Zhaoguo, Z., Hongwei, X., Kaiting, X., Boyang, W., (2024), Analysis and experiment on drag reduction characteristics of digging shovel of *Panax notoginseng* harvester, *Nongye Jixie Xuebao/Transactions of the Chinese Society of Agricultural Machinery* Vol. 55, no.7.

[4] Feng, W., (2022). *Design and experiment of double-layer flat screen tuber harvester for Pinellia ternata*. Master's Thesis, Gansu Agricultural University, Gansu/China.

[5] Guiyun, S., and Ying, L., (2012), Processing, Production and Identification of Orally Taken *Panax notoginseng* Powder, *Capital Medicine (Chuan Tong Zhong Yi Yao)*, no.9, pp. 45—45,

[6] Guo Jingjing, Lailai, L., Huichao, Z., Yang, X., (2014), Research Progress on the Main Components of *Panax notoginseng* and Their Immunomodulatory Effects, *Journal of Tianjin University of Traditional Chinese Medicine* Vol. 33, no.2, pp. 119—124, 0.11656/j.issn.1673-9043.2014.02.17.

[7] Hongwei, X., (2024). *Research on Digging and Conveying Separation Device for Self-propelled Panax Notoginseng Combine Harvester*. Master's Thesis, Kunming University of Science and Technology, Kunming/China.

[8] Issa, I. I. M., Zhang, Z., El-Kolally, W., Wang, F.A., Wang, Y., (2025a), Innovated design, simulation and evaluation of potato harvester excavation and separation conveyors, *International Journal of Agricultural and Biological Engineering* Vol. 18, no.2, pp. 132-145, DOI: 10.25165/j.ijabe.20251802.9164.

[9] Issa, I. I. M., Zhang, Z., El-Kolaly, W., Yang, X., Wang, H., (2020), Design, ansys analysis and performance evaluation of potato digger harvester, *International Agricultural Engineering Journal* Vol. 29, no.1, pp. 60-73,

[10] Issa, I. I. M., Zhang, Z., Omer, A. A. A., Kaiting, X., Zhuma, G., (2025b), A Comprehensive Review of Harvesting Equipment for Rhizome and Tuber Crops: A Bibliometric and Thematic Analysis of Trends, Influences, Intellectual Structures, and Future Directions, *Revista De La Facultad De Ciencias Agrarias* Vol. 57, no.1, pp. 93-121,

[11] Issa, I. I. M., Zhaoguo, Z., El-Kolaly, W., Faan, W., (2025c), Design, Simulation Analysis, and Experiment on Excavation Device of Self-Propelled Panax Noto-ginseng Combine Harvester, *AMA, Agricultural Mechanization in Asia, Africa and Latin America* Vol. 56, no.9, pp. 384-407, DOI: 09.13658/Ama.28.09.2025.01

[12] Jiang, D., Liu, Y., Lin, Z., Wang, W., (2022), Effects of combined infrared and hot-air drying on ginsenosides and drying characteristics of *Panax notoginseng* (Araliaceae) roots, *International Journal of Agricultural and Biological Engineering* Vol.15, no.1, pp. 267-276, DOI: 10.25165/j.ijabe.20221501.6210

[13] Lihong, L., Ying, L., Fen, W., Shilei, L., Huize, H., Wensheng, Z., Wenfeng, X., (2017), The Current Development Situation and Suggestion of Panar notoginseng in Yunnan Pronince, *Modern Chinese Medicine* Vol. 19, no.9, pp. 1331-1335,

[14] Lin, Y., Zhang, F., Li, L. X., Shi, L., Zhu, Y., Wang, J., (2022), Identification of *Panax notoginseng* powder in different parts based on the electronic nose and time-domain feature extraction, *Journal of the Electrochemical Society* Vol. 169, no.4, pp. 047510, DOI: 10.1149/1945-7111/ac62bf.

[15] Siwei, G., (2024). *Research on The Whole Machine Monitoring and Control System of Self-propelled Panax notoginseng Combine Harvester*. Master's Thesis, Kunming University of Science and Technology, Kunming/China.

[16] Thomas, A., (1992), Agricultural water balance of Yunnan Province, PR China: agroclimatic zoning with a Geographical Information System, *Agricultural water management* Vol. 21, no.4, pp. 249-263,

[17] Wang, F., Wen, B., Xie, X., Xie, K., Guo, S., Zhang, Z., (2023a), Operation mechanism analysis and parameter optimization of conveying and separating device of *Panax notoginseng* harvester, *Trans. Chin. Soc. Agric. Mach* Vol. 54, pp. 201-211,

[18] Wang, L., Sun, W., Zhang, L., Zhao, M., and Simionescu, P. A., (2025), Design and Testing of a Self-Propelled Fork-Tooth Harvester for Medicinal Plant Rhizomes, *Agriculture* Vol. 15, no.7, pp. 694,

[19] Wang, L. H., Liu, F., Wang, Q., Zhou, J. Q., Fan, X. Y., Li, J. R., Zhao, X., Xie, S. S., (2023b), Design of a spring-finger potato picker and an experimental study of its picking performance, *Agriculture* Vol. 13, no.5, pp. 945, https://doi.org/10.3390/agriculture13050945.

[20] Wang, W., Yang, R., Pan, Z., Qing, Y., Zhang, J., Chen, D., Guo, X., Lyu, S., (2023c), Design and experimental study of single plant harvester for potato breeding experiments, *Agriculture* Vol. 14, no.1, pp. 71,

[21] Xiaohong, X., (2023). *Experimental Study on Transportation and Separation of Panax Notoginseng Soil Complex*, Kunming University of Science and Technology.

[22] Yitao, L., Chengliang, L., Qingxi, L., Lei, W., (2020), Research progress of seed guiding technology and device of planter, *Nongye Jixie Xuebao/Transactions of the Chinese Society of Agricultural Machinery* Vol. 51, no.12, pp. 1-14,

[23] Zhang, Z., Wang, F., Zhang, Y., Zhang, D., Tian, R., (2016), Design and Experiment of Self-propelled *Panax notoginseng* Harvester, *Journal of Agricultural Machinery* Vol.47, no.1, pp. 234-240, 10．6041/j issn．1000-1298． 2016． S0．036.

[24] Zhaoguo, Z., Haiyi, W., Yanbin, L., Xi, Y., Issa, I., Zhendong, Z., (2021), Design and experiment of multi-stage separation buffer potato harvester, *Nongye Jixie Xuebao/Transactions of the Chinese Society of Agricultural Machinery* Vol. 52, no.2, pp. 96-106,

[25] Zhaoguo, Z., Hongwei, X., Haotian, X., Chang, N., Chao, W., (2023), Calibration and experiment of discrete element parameters of *Panax notoginseng* stem, *Transactions of the Chinese Society for Agricultural Machinery* Vol. 54, no.11, pp. 61-70, 91,

[26] Zhenmeng, C., Zhaoguo, Z., Faan, W., Dan, Z., Haihui, Y., (2018), Kinematic analysis and optimal design of vibration-type device for *Panax notoginseng* root-soil separation, *Journal of Northwest A&F University (Natural Science Edition)* Vol. 46, no.11, pp. 146-154,

[27] Zhongcai, W., Guoliang, S., Xueqiang, L., Faming, W., Chuanzhu, S., Pengxiang, M., (2020), Parameter optimization and test of potato harvester wavy sieve based on EDEM, *Nongye Jixie Xuebao/Transactions of the Chinese Society of Agricultural Machinery* Vol. 51, no.10, pp. 109-122,

[28] Zhou, J., Ye, Z., Cui, X., Zeng, J., Zhao, A., Zhu, L., (2010), Study on the pharmacodynamics of notoginsenosides R1, R2 and ginsenoside R b1 *Chinese Patent Medicine* Vol. 32, no.09, pp. 1494-1497.